Grazing Behavior of Scatter and Propagation Above Any Rough Surface

Donald E. Barrick

***Abstract*— At grazing, propagation and scatter become inextricably connected. For sufficiently low source/observer heights, free-space inverse-distance propagation no longer applies and plane-wave descriptions of scatter give way to surface-wave modes. Concepts like surface radar cross section must be reinterpreted; lack of awareness of these facts in attempts to correlate measurements with grazing-angle laws has led to contradictions. When plane-wave depictions hold, a regime is entered where backscatter follows a grazing angle-to-the-fourth power dependence for surfaces of any roughness scales for both polarizations and for perfectly conducting as well as impedance boundaries above penetrable media. Propagation is described in terms of a roughness-modified effective impedance/admittance that approaches a constant at grazing for all roughness profiles. These facts are first explored with numerical examples, after which we establish universal laws that confirm these suspicions. We derive expressions for the first Taylor-series expansion terms for scatter and impedance/admittance versus grazing angle. Statistics are neither required nor excluded—the laws hold for single arbitrary deterministic profiles as well as averages over ensembles of random surface samples. Proofs of these claims are based on two-dimensional (2-D) fields over one-dimensional (1-D) impedance/admittance boundaries.**

***Index Terms*—Electromagnetic scattering, rough surfaces.**

I. Introduction

As GRAZING is approached above any arbitrary rough surface, physical concepts like propagation and scatter become interrelated; it is difficult to isolate one from the other. Although solutions are often derived (and may be exact) for the scatter response to an incident plane wave, these free-space plane wave depictions may not suffice to describe how energy gets from the radar to and from the scattering cell. Descriptions of radar scenarios involving both propagation and scatter often lead to contradictions, as illustrated below. Clearly a unifying treatment is in order. It should be possible to find limiting relations that apply for both propagation and scatter from *any surface* if one properly separates the relevant interactions.

Consider the following quandary: HF/VHF scatter from the sea; its roughness is simple, it has a continuous single-valued surface, its average slopes are small. Sea water is a good—but not perfect—conductor (at 30 MHz, its Brewster angle is $\sim 1.17^\circ$ above grazing). At HF, its root mean square (rms) heights are small in terms of wavelength and perturbation theory should provide convergent and accurate results. For vertically polarized backscatter (VV), perturbation theory predicts a rapid fall-off with grazing angle—this behavior being evident near and below the Brewster angle. Yet dozens of coastal, commercial HF current-mapping radars view the sea with VV polarization above, at, and below the Brewster angle—even tens of kilometers beyond the horizon where grazing angle is meaningless. In some cases, the observed backscatter coefficientσ° is the classic value for a "perfectly conducting" sea, which the water is not. In other cases, σ° is lower than this value, but still finite rather than the predicted zero value. What has happened? And, if conventional predictions appear to fail at HF (where they are amenable to perturbation solution), why should we assume we can apply concepts of free-space plane waves and derived or measured values of σ° at UHF or X-band near grazing? Surely there is no single radar frequency above which these quandaries suddenly disappear.

This state of disarray is reflected in the literature, where the number of mutually contradictory claims is myriad for grazing propagation and scatter. Perturbation theory results (strictly valid only for small-scale roughness whose height is much less than a wavelength) show grazing angle to the fourth power (α^4) for backscattered energy (plane wave incidence) for both polarizations when the surface is finitely conducting, but α^0 for vertical polarization when the surface is perfectly conducting [1], [2]. Kim and Stoddart [3] note the problems with perturbation theory for VV scatter from perfectly conducting surfaces and conclude that it cannot be used at grazing angles less than 10°. Yet Barrick uses it heuristically to explain quite precisely grazing measurements at HF for both propagation [4] as well as scatter [5] above the sea. Tatarskii and Charnotsii [6] present a derivation for perfectly conducting surfaces, obtaining α^4 for HH and α^0 for VV, claiming this holds for any roughness scale (including perturbation [3] as a subset). Voronovich [7], on the other hand, finds theoretically that α^2 describes backscatter when small roughness waves ride on a large-scale surface with curvature, either concave or convex, regardless of surface medium properties; when the underlying surface is flat, however, he finds that backscatter reverts back to α^4 behavior. Shaw *et al.* [8] use a Kirhhoff theory derivation to predict α^2 dependence for VV backscatter but α^4 for HH. Thus, one has nearly every imaginable permutation of power-law dependence on grazing angle. Unfortunately, measurements by various investigators (e.g., [2], [9]–[12]) of grazing-angle dependence also span the spectrum of power laws, α^n, claiming noninteger as well as integer values for n. Nearly every theoretical study manages to find one set of measurements that are cited to

Manuscript received April 10, 1997; revised September 16, 1997. This work was supported in part by DARPA contract DAAHOL-96-C-R17L and by NOAA's Environmental Research Laboratory under Dr. S. Clifford.

The author is with CODAR Ocean Sensors, Los Altos, CA 94024 USA.

Publisher Item Identifier S 0018-926X(98)01035-7.

support that prediction. And finally, none of these results answers the question raised earlier—what value of grazing angle and/or power law should be used for VV backscatter in the simple case of HF surface wave radar scatter from beyond the horizon?

Propagation near a rough surface (the sea being the most ubiquitous example) is equally beset by quandaries. Ignoring atmospheric refractive effects, derivation of propagation normally begins with an electromagnetic boundary condition for a locally plane interface. An impedance or admittance boundary condition is appropriate when the medium below the interface is dense/conducting, as is the sea below K_a-band. Conventional derived models that cast the interaction in terms of a space wave (direct and reflected rays) and surface wave often express the Fresnel specular reflection coefficients and surface wave asymptotics in terms of an effective surface impedance or admittance (Wait [13], [14]). Feynberg [15] followed by Barrick [4] showed that roughness on the locally plane interface "modifies" the value of the lower medium impedance and derived specific values for this effective VV impedance for the sea at HF using perturbation theory. These results produce an effective impedance that is independent of grazing angle in the limit, resembling the impedance or admittance for a flat surface above an homogeneous medium in this respect.

Modern numerical methods such as the Fourier split-step solution of the parabolic wave equation (Dockery and Kuttler [16]) that include the atmosphere require estimates for the surface impedance. Above HF, for lack of a better model, the "Miller–Brown" optics result [17] has been used for both VV and HH propagation. This simple model essentially multiplies the Fresnel smooth-surface reflection coefficient by an exponential "Rayleigh roughness factor." Resulting impedances and admittances at X-band, for example, then become highly dependent on grazing angle. Yet this disappointingly reduces the desirability of an approach like the split-step algorithm, which implicitly bypasses the complexity of ray-trace modeling that carries along the angles of each ray. The Miller–Brown approach requires an independent method of estimating the grazing angle for a different impedance at each range step of the algorithm. Not only is this cumbersome, but it defies sense and intuition: there has never been any evidence (theoretical or experimental) that the roughness-modified surface impedance should be angle-dependent near grazing at any frequency.

Barrick [18] presented a unified modal approach to propagation and scatter above a one-dimensionally (1-D) rough surface describable by an impedance/admittance boundary like the sea. Inherently exact, the only approximation introduced is the truncation of an infinite set of equations to solve for the fields at the surface. Unlike moment methods, these surface fields/currents are expressed as Fourier harmonic coefficients of some arbitrary surface period. The method obtains results for both scatter and propagation. Scatter arises from re-radiation by surface currents/fields, while a roughness-modified effective impedance/admittance is included in the specular (or forward) mode. Numerical solutions with this method sometimes become unstable because of ill-conditioned matrix inversion at very high frequencies and/or at steep surface slopes.

Examples from this approach suggest that for sea-like roughnesses at frequencies well above HF (up to 500 MHz), the following "grazing laws" appear to hold for impedance/admittance rough boundaries (of which perfectly conducting surfaces are a limiting subset).

1) Backscattered power depends on grazing angle to the fourth power (α^4) for both polarizations regardless of frequency, roughness details, underlying curvature, surface material, surface statistics, even whether or not the power is averaged.
2) The roughness-modified impedance and admittance tend to constants as grazing angle is approached for both polarizations.
3) For surface scales sufficiently large in terms of wavelength, a roughness-dependent "Brewster-angle" dip in the effective Fresnel reflection coefficient appears for HH polarization as well as VV, even for perfectly conducting surfaces.

We demonstrate these claims in Sections II and III with numerical solutions for surfaces with ocean-type roughness statistics. Prodded by these numerical examples, we then employ Barrick's [18] formulation in Section IV to establish general laws for backscatter and the modified impedance/admittance near grazing. Numerical solution of specific surface examples is not required to arrive at our power-law dependences, thereby bypassing any equation-set truncation approximation and/or matrix ill-conditioning inconveniences. Nor do we need to assume arbitrary statistical properties or even averaging. Our resulting general laws validate the three grazing-angle features noted above.

Arrayed with these tools, in Section V, we revisit the quandary presented earlier: nonvanishing VV backscatter from the sea for coastal HF radars. A perturbation reduction of our modal approach in the Appendix is applied to this example, allowing us to define a radar cross section for surface wave propagation (the actual source may be below the horizon where plane wave incidence and "negative" grazing angle have no meaning).

II. Grazing Scatter Examples from Sea-Type Surfaces

We consider examples of backscatter near grazing by numerically solving for random sea-like profiles using the modal approach of Barrick [18]. These will illustrate the trends versus grazing angle that spur our general attack of Section V.

A. The Modal Formulation for a Periodic Profile

We briefly review the essential equations derived in [18] to treat VV and HH interaction with 1-D rough surfaces. The equations below modify and improve on some indexing inconsistencies in the original work [18]. Let f_y represent the y-directed component of the H-field for VV polarization or the E-field component for HH polarization, where propagation is contained in the x–z plane. For a plane wave with wavenumber k incident on the periodic surface $\zeta(x)$ with fundamental wavenumber $\kappa = 2\pi/L$ (L is spatial period) at grazing angle

α from the $-x$ direction, the incident field is represented by

$$f_y^i = e^{-ik\cos\alpha x - ik\sin\alpha z - i\omega t} \tag{1}$$

where we, henceforth, omit the time dependence. The y-directed component of the scattered field modes is then given by

$$f_y^s = \sum_{n=-\infty}^{+\infty} F_n e^{in\kappa x - ik\cos\alpha x + i\kappa_n z}, \qquad \text{for } z > \zeta_{\text{Max}} \tag{2}$$

where, for a surface satisfying impedance/admittance boundary conditions, the coefficients (modal scattering amplitudes) F_n are solutions to the exact equation sets

$$[P_{mn}]\,[S_n] = [2\sin\alpha\,\delta_m^0] \tag{3a}$$

and

$$[Q_{mn}]\,[S_n] = [2\chi_m F_m]. \tag{3b}$$

The unknown surface-field Fourier coefficient vector S_n is found from solving (3a) and inserting this into (3b), where the infinite systems of equations represented in (3) are truncated, as discussed in [18]. Here, δ_m^0 is the Kronecker delta function (equal to one only when $m = 0$) and the vector/matrix indexing runs over positive and negative integers for propagating and evanescent modes, respectively. The known input matrices required in (3) are given by

$$\begin{aligned} P_{mn} &= \left[\frac{1-\xi_m\xi_n}{\chi_m} + \mathtt{z}\right]\cdot p_{n-m}^m \\ Q_{mn} &= \left[\frac{1-\xi_m\xi_n}{\chi_m} - \mathtt{z}\right]\cdot q_{n-m}^m \end{aligned} \qquad \text{Vertical Polarization} \tag{4a}$$

$$\begin{aligned} P_{mn} &= \left[\frac{1-\xi_m\xi_n}{\mathtt{y}\chi_m} + 1\right]\cdot p_{n-m}^m \\ Q_{mn} &= \left[\frac{1-\xi_m\xi_n}{\mathtt{y}\chi_m} - 1\right]\cdot q_{n-m}^m \end{aligned} \qquad \text{Horizontal Polarization} \tag{4b}$$

where

$$\xi_m \equiv \cos\alpha - \frac{m\kappa}{k}, \quad \chi_m \equiv \sqrt{1-\xi_m^2} \quad \text{and} \quad \kappa_m \equiv k\chi_m. \tag{4c}$$

The quantities z and y are the normalized impedance and admittance at the rough boundary. For a homogeneous lower medium of relative complex dielectric constant ε, they apply when $|\varepsilon_r| \gg 1$, in which case they become

$$\mathtt{z} = \frac{\sqrt{\varepsilon_r - \cos^2\alpha}}{\varepsilon_r} \quad \text{and} \quad \mathtt{y} = \sqrt{\varepsilon_r - \cos^2\alpha}. \tag{4d}$$

The shape and/or statistics of the rough surface profile is contained in the modal Fourier expansion of the surface characteristic function, defined as

$$e^{i\kappa_m\zeta(x)} = \sum_{j=-\infty}^{+\infty} p_j^m e^{-ij\kappa x} \quad \text{from which}$$
$$p_j^m = \text{IFFT}_j(e^{i\kappa_m\zeta(x)},\, N) \tag{5a}$$

$$e^{-i\kappa_m\zeta(x)} = \sum_{j=-\infty}^{+\infty} q_j^m e^{-ij\kappa x} \quad \text{from which}$$
$$q_j^m = \text{IFFT}_j(e^{-i\kappa_m\zeta(x)},\, N) \tag{5b}$$

where $\text{IFFT}_j(g,\, N)$ denotes the standard IEEE inverse N-point fast Fourier transform of function g whose output is arrayed as a vector over index "j." As a check, when the profile is sinusoidal $\zeta(x) = A\cos(\kappa x)$, then the modal surface coefficients become the familiar cylindrical Bessel functions $p_j^m = i^j J_j(\kappa_m A)$.

B. Far-Field Scatter from a Finite-Length Observation Cell

Far-field scatter from the roughness profile inside a finite radar cell (e.g., pulse limited) of length L is treated as follows. First, this cell profile is repeated at intervals L, making the surface periodic with fundamental wavenumber $\kappa = 2\pi/L$. Then the exact modal scattered field of (2) along a strip at height z_r above the highest point on the profile is substituted into a two-dimensional (2-D) far-zone radiation or aperture integral (for example Holliday's *et al.* (30) [25]), which is valid when $r \gg 2(\sin\beta L)^2/\lambda$

$$F_y^s(\boldsymbol{r}) = \frac{i}{4}\sqrt{\frac{2}{\pi kr}}\, e^{i(kr - 3\pi/4)} \int_{-L/2}^{+L/2} dx(\boldsymbol{k}^s \times \hat{x}) \cdot f_s^y\, e^{ikx\cos\beta - ikz_r\sin\beta} \tag{6a}$$

where $\boldsymbol{k}^s = (k\cos\beta,\, k\sin\beta)$ is the radio wavevector pointing in the scatter direction β, which, like α, is measured from the $-x$ axis. Substituting the modal scattered field of (2) into (6) and integrating gives

$$F_y^s(\boldsymbol{r}) = \frac{i}{4}\sqrt{\frac{2}{\pi kr}}\, e^{i(kr-3\pi/4)} kL\sin\beta \sum_n F_n \cdot \frac{\sin(n\kappa - k\cos\alpha + k\cos\beta)\dfrac{L}{2}}{(n\kappa - k\cos\alpha + k\cos\beta)\dfrac{L}{2}}\, e^{i(\kappa_n - k\sin\beta)z_r}. \tag{6b}$$

Let us now restrict attention to backscatter where $\beta = \pi - \alpha$ (so $\cos\beta = -\cos\alpha$). For L sufficiently large, the $\sin(x)/x$ function above becomes a Kronecker delta, selecting the integer n^* corresponding to backscatter such that $n^* = (2k/\kappa)\cos\alpha$. Thus, one term remains in the summation—that for $n = n^*$. Finally, we take the absolute square of the field strength and multiply by $2\pi r/L$ to get the dimensionless backscatter width per unit surface length, σ° to obtain

$$\sigma^\circ = kL\,\frac{\sin^2\alpha}{4}|F_{n^*}|^2. \tag{7}$$

This methodology for transforming the modal solution for a periodic surface to far-field scatter from a bounded radar cell has been used since Rice [19] for nearly five decades and produced the first perturbation-limit rough-surface cross sections [1], [2], [4], [20], [21] that are now universally accepted.

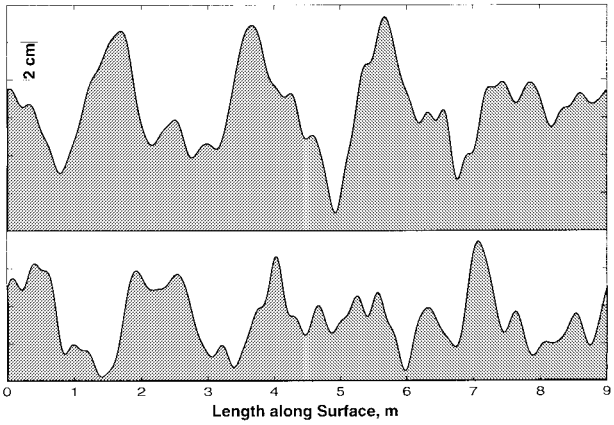

Fig. 1. Samples from random ensemble of sea-surface-like profiles that follow a Phillips spectral law for height spectral density versus spatial wavenumber. Used for Monte Carlo numerical calculations at 500 MHz.

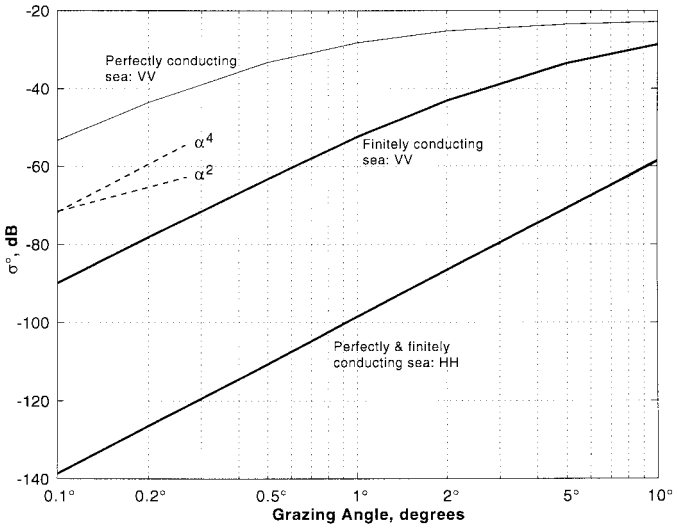

Fig. 2. Results for average normalized backscatter radar cross section from Monte Carlo calculations based on 2048 surface sample profiles resembling Fig. 1. Light curves: perfectly conducting surface; heavy curves: finitely conducting sea water at 500 MHz. Dashed curves at left show slopes corresponding to square and fourth power of grazing angle.

C. Application to Backscatter from Random Sea-Like Profiles near Grazing

We study ensembles of sea profiles using the above methodology by taking a radar frequency of 500 MHz (wavelength 60 cm) and a fundamental period for the sea and our cell of $L \cong 9$ m. As we are considering the region near grazing where $\cos\alpha \sim 1$, we adjust the period L slightly with grazing angle so that backscatter occurs precisely at integer mode $n^* = 30$. The profile is composed of spatial harmonics of the fundamental ($\kappa = 2\pi/L$) that follow a 1-D Phillips spectral model:

$$S(\kappa) = \frac{B}{\kappa^3}, \qquad \text{for } \kappa_c < \kappa < \infty$$

such that

$$h^2 = \int_{\kappa_c}^{\infty} S(\kappa)\, d\kappa = \frac{B}{2\kappa_c^2} \tag{8}$$

where $B = 0.005$ and "h" is the rms sea waveheight. The cutoff κ_c is often given in terms of the surface wind speed for fully developed seas. Since we are dealing with a short piece of sea, we take $\kappa_c = 4\kappa$ and include spectral harmonics describing the profile that range from $n = 4$ to $n = 36$ (beyond backscatter at $n^* = 30$). Each spectral harmonic is a zero-mean Gaussian random variable whose variances are given by (8). Our Monte Carlo modeling includes 2048 profile samples (two typical examples of which are shown in Fig. 1). For each of these surface samples, we vary grazing angle between 10° and 0.1°. Both VV and HH polarization are analyzed.

The sea, of course, is not perfectly conducting. It has a dielectric constant 81 and conductivity 4 mho/m. These are used in (4d) to define the normalized surface impedance and admittance at 500 MHz. For illustrative purposes, we also allow the sea to be perfectly conducting for these same profiles. The backscattered power is then computed and averaged for each of the 2048 surface samples. The resulting normalized backscatter coefficient σ° is shown in Fig. 2.

Light curves show σ° for a perfectly conducting surface, while the heavy curves represent the actual sea impedance/admittance at 500 MHz. The results for HH for the perfectly/finitely conducting cases overlay each other. Also shown as dashed (for reference) are line sections whose slopes correspond to α^4 and α^2 dependences.

When actual seawater properties are used, grazing-angle behavior for $\alpha < 1°$ matches the α^4 dependence for both polarizations. What is surprising is that VV for the perfectly conducting case is clearly tending toward α^4 also, although above 10° it plateaus. Classic perturbation theory (as well as studies of Tatarskii and Charnotskii, [6]) predict a flat response as grazing is approached. Our modal approach is more exact than perturbation theory, although the latter approximation might have been expected to hold here since $kh = 0.178$ for our surfaces. For a perfectly conducting sea whose 1-D spectrum is given by (8), the VV perturbation result at $\alpha = 0°$ is $\sigma^\circ = (\pi/2)B \Rightarrow -21$ dB (see the Appendix), which is close to our Monte Carlo value in Fig. 2 above $\alpha = 10°$ (serving as a check on that method and our modal solution). This tendency toward α^4 provides impetus for the general proofs presented in Section IV establishing this grazing angle dependence as universal rough surface behavior.

D. Does Underlying Curvature Matter?

Voronovich [7] performed a theoretical study that produced two interesting and provocative assertions: 1) Smaller-scale roughness riding on a large-scale profile with a given curvature produces α^2 grazing-angle behavior independent of the value of curvature and 2) the curvature-modified scatter—although different for VV and HH—depends very weakly on whether the profile is convex or concave. He applied this to return at X-band from a sea with a dielectric constant $\varepsilon_r = 51.4 + i39.1$, assuming a 1-D profile as we do herein. We study this in the same manner as the previous example, using Monte Carlo modeling for the small-scale sea waves and superposing them on: 1) a concave surface; 2) a flat surface; and 3) a convex surface. 2048 samples are averaged. Sizes are scaled from the previous 500 MHz example to X-band at 10 GHz (20 : 1). For

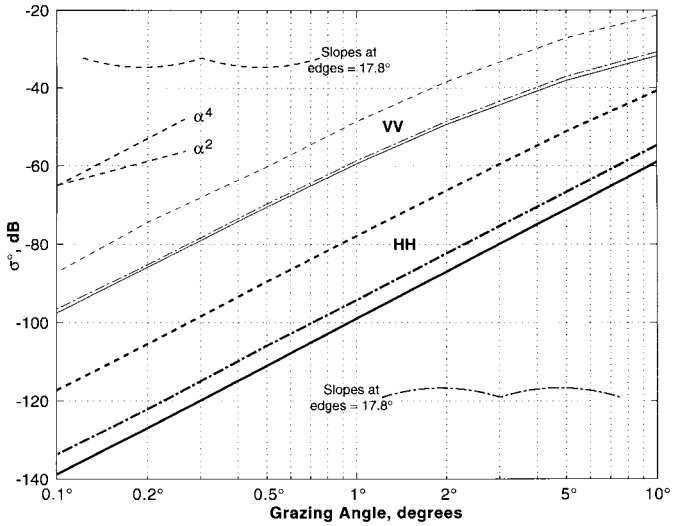

Fig. 3. Backscatter cross sections for sea-like roughness of Fig. 1 superposed on concave (dashed), convex (dash–dot), and flat underlying profiles. Light curves at top are for VV polarization; heavy at bottom are for HH. Short curve segments at left give square and fourth power grazing angle dependence slopes.

comparison, we employ a circular arc with a normalized radius of curvature $R/\lambda = 24.5$, as did Voronovich. To preclude significant near-grazing shadowing, we set the period to be 45 cm; slopes at the cell edges are then 17.8°. In the cases of added convex and concave curvature $kh = 2.32$, so that those surfaces are not treatable by perturbation theory; with no curvature $kh = 0.18$, so perturbation theory should apply. In our numerical matrix inversion, condition numbers always stayed within six decimal digits of machine precision and results were checked for energy conservation. Fig. 3 plots of the output.

We find that all averaged calculated values for σ° tend toward α^4 rather than α^2. VV polarization always has higher values than HH. Finally, concave surfaces produce higher backscatter than convex (as seems intuitive), by 10 dB for VV to 15 dB for HH. Zero curvature gives even slightly lower power than the convex profile. This provides yet another example suggesting a universal trend to α^4 at grazing.

III. Grazing Propagation Examples from Sea-Type Surfaces

As the incident plane-wave approaches grazing ($\alpha \Rightarrow 0$), difficulties encountered with backscatter—especially for VV polarization—appear also in the forward direction.

A. Specular Reflection at a Planar Interface

When field components lie perpendicular to the plane of incidence (the page), the Fresnel reflection coefficients for VV (H-field perpendicular) and HH (E-field perpendicular) at a planar impedance/admittance boundary become

$$R_v(\alpha) = \frac{\sin\alpha - \mathtt{z}}{\sin\alpha + \mathtt{z}}, \quad \text{and} \quad R_h(\alpha) = \frac{\sin\alpha - \mathtt{y}}{\sin\alpha + \mathtt{y}}. \qquad (9)$$

For a sea-type conducting medium, the normalized impedance $\mathtt{z}$ is always much less than unity, while the admittance $\mathtt{y}$ is correspondingly greater than unity [the two are nearly reciprocals of each other—(4d)]. Hence, R_h is always negative and close to -1 for any grazing angle α. For R_v, there is some α at which the numerator is minimum; this is called the *Brewster angle*. Above this angle, R_v is close to $+1$ for small $\mathtt{z}$, but as grazing is approached below the Brewster angle, R_v tends to -1 just like HH polarization.

Suppose we define from the outset the surface as perfectly conducting: a Neumann boundary for VV. This makes $\mathtt{z} = 0$ so that $R_v = +1$ *for all* α even down to grazing. If, however, one admits even an infinitesimal $\mathtt{z}$ (making the surface almost perfectly conducting), the above equation shows that $R_v \Rightarrow -1$ as $\alpha \Rightarrow 0$. Does it not seem a bit more than coincidental that a very similar behavior attends VV backscatter σ° as grazing is approached when one tries to bridge the seeming gap between the constant α^0 dependence for perfectly conducting surfaces and the α^4 behavior for finite but very small $\mathtt{z}$? No such differences appear for horizontal polarization between perfect and finite conductivity in both the scattering and propagation cases, and for small $\mathtt{z}$ (large $\mathtt{y}$), both are nearly identical in their behavior from $\pi/2 > \alpha > 0$.

Feynberg [15] was first to note that slight roughness on an otherwise perfectly conducting plane increases the impedance $\mathtt{z}$ from zero to a finite amount, thereby emulating the behavior of a dielectric/conducting flat interface. Barrick [4] and Rice [19] proceeded further, obtaining expressions for an additive impedance (from perturbation theory to second order) to account for roughness for both perfect and finitely conducting boundaries. Although these perturbation results have a finite radius of convergence (meaning they do not remain valid when roughness height grows beyond the radio wavelength), one might expect a continuation of this general behavior even though one particular mathematical analysis method may no longer apply.

A final phenomenon is noteworthy. As grazing is approached, the sum of direct and reflected rays cancel and the forward field over the surface is extinguished for both polarizations. Remember, one needs only a very small amount of roughness on an otherwise perfectly conducting surface for this to happen for VV and it always occurs for HH. If the total forward-mode field is zero, there is nothing available to excite scatter. Nonetheless, one can propagate energy along a finitely conducting (impedance) surface, especially for vertical polarization; this is known as the surface wave. Clearly, it *is not* describable in terms of a direct and reflected plane wave. Surface-wave models are appropriately formulated in terms of the boundary impedance, $\mathtt{z}$, which exhibits a stable behavior near grazing. This subject is revisited later.

B. Impedance/Admittance at Grazing and Relation to Reflection

Impedance or admittance boundary conditions are defined in terms of the ratio of the field and its normal derivative at the interface. For a planar interface, (9) express the V/H Fresnel reflection coefficient in terms of the impedance/admittance

and the grazing angle. Conceivably, the impedance/admittance could implicitly be a function of grazing angle also, but in practice, these quantities approach a constant value at grazing ($\alpha \Rightarrow 0$). This is seen for a smooth interface over a homogeneous lower medium from (4d) when $\varepsilon_r \gg 1$. The works of Barrick [4] and Feynberg [15] show that the impedance contributed by roughness is also independent of α near grazing, suggesting a universal behavior of $\mathtt{z}$ and $\mathtt{y}$ such that they both tend to constants at grazing. Examples are given below exhibiting this property, followed by a general proof of this suspicion in Section IV for all rough surfaces independent of frequency.

Because an impedance/admittance boundary condition is useful in propagation problems, in particular, the numerical solution of a reduced parabolic version of the wave equation (Dockery and Kuttler, [16]), this grazing-angle dependence (or lack thereof) becomes critical. It has been the practice (for lack of an alternative) to multiply the reflection coefficients of (9) by the "Miller–Brown" factor [17] that supposedly accounts for roughness. This factor is similar to the exponential "Rayleigh roughness factor" that is found in Beckmann and Spizzichino [22], but is multiplied by a zero-order cylindrical Bessel function. Both factors (given below) are based on optics/Kirchhoff scattering models, which are both physically and mathematically untenable for rough surfaces close to grazing (see Voronovich, [7]). Equation (9) is then multiplied by this factor and solved for impedance $\mathtt{z}$ and admittance $\mathtt{y}$, which become highly dependent on grazing angle above VHF as $\alpha \Rightarrow 0$, in contrast with the behavior expected herein

Rayleigh Roughness Factor:

$$\mathrm{Ra} = e^{-2(kh\sin\alpha)^2} \tag{10a}$$

Miller–Brown Roughness Factor:

$$\mathrm{MB} = \mathrm{Ra}\cdot J_0[i2(kh\sin\alpha)^2]. \tag{10b}$$

To study this problem further, we examine 1-D ocean wave profiles at 500 MHz, using the same Monte Carlo modeling approach described in Section II. Here, however, we employ more realistic sea wave statistics: a dominant ocean gravity-wave period of 50 m (spatial) or 5.6 s (temporal). With the Phillips spectral model of (8) to define the variances of the random ocean wave spectral height components, the significant wave height for our 400 surface-sample ensemble averaging turns out to be 4.3 ft (1.3 m). The impedance/admittance for sea water at 500 MHz is used in the modal solutions. Grazing angles below 10° are studied and the impedance/admittance are determined from the specularly reflected mode term (i.e., $R_{v,h} = F_0$) for each polarization using (9) above. The results of the modal theory are shown in Fig. 4 as the heavy curves. For comparison, we plot the impedance/admittance obtained by the Miller–Brown factor multiplying the flat-plane reflection coefficient as the light curves. Note for reference that the impedance and admittance of a smooth interface above sea water from (4d) are $\mathtt{z} = 0.0672 - i0.0390$ and $\mathtt{y} = 11.0625 + i6.5082$ (compared to $\mathtt{z} = 0.0746 - i0.0497$ and $\mathtt{y} = 0.4261 - i0.4374$ from modal theory at $\alpha = 0°$).

First note that at 500 MHz, both the Miller–Brown approximation and the exact modal solution, predict flat behavior with grazing angle for VV. In fact, the two results agree reasonably well, although this good agreement does not continue to hold as one approaches X-band for VV. For HH, however, the agreement is poor. The modal solution result becomes flat but the Miller–Brown results change very rapidly with α. This behavior is not realistic and can only lead to inaccuracies if such an α-dependent admittance is used in numerical modeling of near-surface propagation.

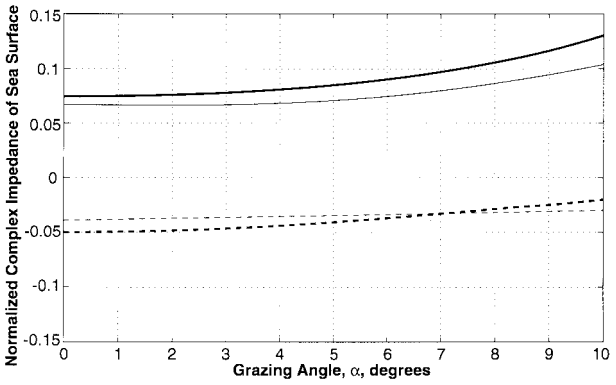

(a)

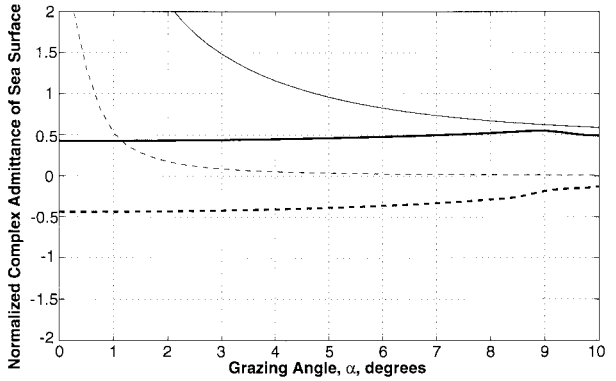

(b)

Fig. 4. (a) Normalized surface impedance for random finitely conducting sea with Phillips spectrum at 500 MHz based on Monte Carlo simulations (400 samples) for vertical polarization. Significant waveheight is 4.3 ft (1.3 m) and dominant period is 50 m (5.6 s temporal period). Solid curves: real part; dashed curves: imaginary part. Heavy curves are calculated from exact modal theory; light curves are Miller–Brown factor applied to flat-plane Fresnel reflection coefficient. (b) Same as (a), but plots normalized surface admittance for horizontal polarization.

Observe that sea state (or roughness) has a moderate effect on impedance at 500 MHz, but produces a dramatic change to the admittance over that for sea water alone. The principal conclusion suggested by these examples is that roughened interfaces modify the effective impedance/admittance, but they both remain flat near grazing.

An interesting observation is that the "roughness-modified" admittance resembles an impedance in that it actually becomes less than unity! If this flat behavior with α persists at higher grazing angles, one will see a "Brewster-angle" dip in $R_h(\alpha)$ as $\sin\alpha$ becomes equal to Real $(\mathtt{y})$ after which the reflection-coefficient phase becomes less than $\pi/2$ as nadir is approached. This phenomenon is uncharacteristic of flat surfaces reflections for HH polarization.

IV. Taylor-Series Expansion of Backscatter and Impedance/Admittance in Grazing Angle

Prodded by the examples above, we demonstrate in this section that the backscattered field and impedance/admittance have Taylor-series expansions in α (grazing angle) that support our claims. This is established for any arbitrary surface profile, lower-medium impedance/admittance (including perfectly conducting interfaces), frequency-roughness scales; it holds whether or not statistical averaging is introduced. The modal matrix formulation of Barrick [18], summarized in Section II, is employed in this proof.

A. Binomial Inversion of Two-Term Taylor Matrix Expansion

The essence of our attack is: 1) to expand all the known matrices and vectors in Taylor series versus grazing angle α; 2) to retain only the lowest two terms in α; and 3) to solve for the desired backscattered field and impedance/admittance dependence on α by a simple binomial expansion for the required matrix inversion.

The unknown quantities that are the heart of the proof are the fields or equivalent currents on the surface. These are represented by the vector S_n in (3), which are the harmonic coefficients of these currents written as a Fourier series over the fundamental spatial period of the surface profile. First, we note that these coefficients exist because the surface field exists. Furthermore, in practice, only a finite number of these are appreciably different from zero. They fall off rapidly in magnitude at spatial harmonics beyond twice the radio wavenumber because rapid variation of currents/fields on spatial scales much less than a wavelength is difficult to excite with an incident plane wave. Hence, in principle, both the forward version and the inverse versions of (3a) exist and are exact; we rewrite these here (for brevity) as

$$[P][S] = 2[E] \ \text{(direct)}, \quad [S] = [P]^{-1}2[E] \ \text{(inverse)} \tag{11}$$

where the excitation vector E contains only one element: $\sin\alpha$ at the $m = 0$ position.

Expand the matrices P and E of (11a) in Taylor series in α (i.e., expand every matrix element thusly), retaining terms through first order in α and writing them as

$$\{[P_0] + [P_0']\alpha\}[S] = 2[E_0']\alpha \tag{12}$$

where prime means differentiation with respect to α, and the "0" subscript means $\alpha = 0$ has been substituted into the result. It is evident from (3a) that the right side is linear in grazing angle, with $E_0' = \delta_m^0$.

We now find an expression for the inverse $[P]^{-1}$ through first order in α. We do this by analogy with the scalar binomial expansion. In the equation $(p + q\alpha)r = 1$, r is the inverse of $(p + q\alpha)$, i.e., $r = (p + q\alpha)^{-1}$. In the small-α limit, this becomes $r \cong p^{-1}(1 - \alpha/p) + O(\alpha^2)$. Cast in that form, it elucidates its matrix counterpart (below)

$$[P]^{-1} \cong [P_0]^{-1} - [P_0]^{-1}[P_0'][P_0]^{-1}\alpha + O(\alpha^2). \tag{13}$$

The easiest way to convince oneself of this relation is to multiply it by the P-expansion factor on the left side of (12), thereby obtaining the identity matrix to second order in α.

Substitute this into (11b) to obtain the surface field mode-coefficient vector S_n and then into (3b) with Q similarly expanded through first order to obtain the scattered-field mode-coefficient vector F_m

$$[S] \cong 2\{[P_0]^{-1} - [P_0]^{-1}[P_0'][P_0]^{-1}\}[\delta_m^0]\alpha \tag{14}$$

$$[\chi F] \cong ([Q_0][P_0]^{-1} + \{[Q_0'][P_0]^{-1} - [Q_0][P_0]^{-1}[P_0'][P_0]^{-1}\}\alpha)[\delta_m^0]\alpha. \tag{15}$$

Observe that only one matrix inverse is required: $[P_o]^{-1}$. We need not worry how to find this inverse numerically or its size for now—only that it exists. It exists because the surface-field vector F_m exists as discussed above and is defined by (11). Our formulation is still general so it can apply to any surface profile. *Our claims will be proven based on (14) and (15).*

B. Particulars of the Angle-Independent Taylor-Series Matrices

1) Forward/Backscatter Geometry Symmetry Adjustment: With no sacrifice in generality, we choose the fundamental period near grazing so the backscatter direction is represented by an *integer* mode, i.e., at index $m^* = 2k\cos\alpha/\kappa$. Let the number of elements in our square matrices be odd so that a nadir scattered mode at $m^*/2$ bisects the forward mode at $m = 0$ and the backscatter mode at $m = m^*$. Forward and backscatter now have a useful symmetry about the nadir.

2) Grazing-Limit Matrix Values:

a) The P_0, Q_0 matrices: All elements of these matrices are easily obtained by setting $\alpha = 0$ in the defining (4) and (5), *except* for the $m = 0$ *and* $m = m^*$ *rows*. Here, one must take limits of both numerator and denominator in (4) because $\chi_0 = \chi_{m^*} = \sin\alpha \Rightarrow \alpha \Rightarrow 0$. These terms then become

$$P_0|_{m=0} = \begin{cases} -iknz_{-n} + \mathtt{z}\delta_n^0 \ \text{(VV)} \\ -iknz_{-n}/\mathtt{y} + \delta_n^0 \ \text{(HH)} \end{cases}$$

and

$$Q_0|_{m=0} = -P_0|_{m=0} \tag{16}$$

where z_n and ν_n are Fourier coefficients of the surface profile height and its square

$$\zeta(x) = \sum_{n=-\infty}^{+\infty} z_n e^{in\kappa x} \quad \text{and} \quad \zeta^2(x) = \sum_{n=-\infty}^{+\infty} \nu_n e^{in\kappa x}. \tag{17}$$

Owing to our forward/back symmetry, the $m = m^*$ row of P_0 is obtained in the following way: 1) centered on the $n = n^*$ element, pivot the $m = 0$ row backward around its $n = 0$ element; 2) in place of the first term $-iknz_{-n}$ above, use $+iknz_{-n}^*$; and 3) negate the second term with δ_n^0 above. The Q_0 row for m^* is the negative of that for P_0, like (16b) above.

b) The P_0', Q_0' derivative matrices: All elements of these matrices are identically zero except the $m = 0$ and the $m = m^*$ rows. The elements of the $m = 0$ row are

$$P_0'|_{m=0} = Q_0'|_{m=0}\begin{cases} \delta_n^0 - k\kappa n\nu_{-n}/2 + ikz_{-n}\mathtt{z} \ \text{(VV)} \\ \delta_n^0 - k\kappa n\nu_{-n}/2\mathtt{y} + ikz_{-n} \ \text{(HH)} \end{cases}. \tag{18}$$

The $m = m^*$ row elements are obtained by the same symmetry pivoting described above, but taking complex conjugates of the first term $k\kappa n\nu_{-n}/2$.

3) The Forward and Backscattered Modes: We study only two of the scattered mode coefficients derived in (15): F_0 and F_{m^*}. In this limit, the χ multiplying both F_0 and F_{m^*} on the left side of (15) becomes α, canceling the α-factor common to the right side

$$F_{0 \text{ or } m^*} \cong \{[Q_0][P_0]^{-1}\}_{n=0 \text{ column}}^{m=0 \text{ or } m^* \text{ row}} + \alpha\{[Q_0'][P_0]^{-1} - [Q_0][P_0]^{-1}[P_0'][P_0]^{-1}\}_{n=0 \text{ column}}^{m=0 \text{ or } m^* \text{ row}}. \quad (19)$$

Hence, proof of our claims lies in establishing the following values for the first term in the above equation: 1) it is -1 for $m = 0$ (forward/specular scatter) and 2) it is 0 for $m = m^*$ (backscatter). We do this in two ways—by mathematical proof and by physical arguments that elucidate the merging of propagation and scatter in the grazing limit.

a) Mathematical proof: If the first matrix factor Q_0 had been P_0, the product representing the first term would be the identity matrix by definition. In this case, the (0, 0) element is the diagonal value $+1$ and the (m^*, 0) off-diagonal element is zero. In fact, however, the $m = 0$ and $m = m^*$ rows of the Q_0 matrix are identical—but with elements negated—from these same rows of the P_0 matrix as demonstrated in (16b), above. Hence, the contribution to F_0 is -1, and the contribution to F_{m^*} is 0.

b) Physical proof/interpretation: Note from (14) that the surface fields/currents, as represented by their Fourier mode coefficients S_n go to zero in the grazing limit because they are directly proportional to α. This is true for *all* modes n for both polarizations, regardless of whether the surface is perfectly or finitely conducting. If these surface fields are zero, then the scattered or reradiated fields they produce must be zero. This demands all F_n (for $n \neq 0$, including the F_{n^*} backscatter mode) go to zero at least as fast as α. So what happens to the incident plane wave field with defined unity amplitude as grazing is approached? It is extinguished upon combination with the forward reflected mode F_0, which, therefore, must have -1 amplitude. This is exactly what happens near any flat interface above a homogeneous medium at grazing for either polarization: the Fresnel reflection coefficient becomes -1, canceling the incident plane wave. As shown by Feynberg [15], slight roughness on a perfect conducting plane also produces a small effective surface impedance accompanied by a Fresnel coefficient that must go to -1 at grazing. Hence, the same near-grazing behavior grazing is caused by roughness on the interface as well as nonperfect electrical properties of the lower medium.

4) Backscatter Behavior at Grazing: Since we have proven that the first term of (19) vanishes, we can write the normalized backscattering width of (7) as

$$\sigma_{back}^{\circ} \Rightarrow kL\,\frac{\alpha^4}{4}|\{[Q_0'][P_0]^{-1} - [Q_0][P_0]^{-1}[P_0'][P_0]^{-1}\}_{m^*,\,0}|^2 \quad (20)$$

establishing our claim of grazing-angle-to-the-fourth dependence for backscatter from all rough interfaces.

5) Effective Surface Impedance/Admittance at Grazing: Note that F_0 (the mode in the forward direction) is identically the Fresnel reflection coefficient above a plane that includes the roughness. By inspection of the classic planar Fresnel coefficient of (9), we define a *new* normalized effective impedance/admittance Z, Y at grazing ($\sin\alpha \Rightarrow \alpha$)

$$Z, Y = \alpha\,\frac{1 - F_0}{1 + F_0}. \quad (21)$$

The first term of F_0 from (19) is -1, which negates the $+1$ in the denominator so that its remaining α dependence cancels the multiplicative α; the numerator becomes $+2$ in the limit $\alpha \Rightarrow 0$ so that

$$Z, Y = \frac{2}{\{[Q_0'][P_0]^{-1} - [Q_0][P_0]^{-1}[P_0'][P_0]^{-1}\}_{0,\,0}}. \quad (22)$$

Hence, the result that the impedance/admittance is always constant in the grazing limit.

C. Where Does the Grazing Regime Begin?

How close to grazing must one be before the limiting expressions derived above apply? Consider two cases.

1) When the modulus of Z, Y is less than unity, a transition occurs near a "pseudo-Brewster angle" at $\alpha \cong arc\sin(|Z, Y|)$. At angles greater than this value, the interactions resemble VV above a homogeneous medium: the Fresnel specular reflection has positive phase and the backscattered power is flat versus α, as paradoxically predicted by perturbation theory above perfectly conducting surfaces [1], [3], [5], [6]. At values of α much lower than our pseudo-Brewster angle, the reflection coefficient phase tends to 180° and backscattered power decays as α^4.
2) The case where the modulus of Z, Y is greater than unity resembles HH over homogeneous media, with the Fresnel reflection phase always negative over the upper half space. When Z, Y is much greater than unity, backscattered power tends to a $\sin^4\alpha$ law everywhere.

V. Resolution of HF Sea-Scatter Paradox for VV: The Surface Wave

Why does the sea appear to defy the α^4 law set forth above, disagreeing also with perturbation theory for VV backscatter from a finitely conducting surface at grazing? The reason has to do with the use of plane waves to represent the radiated field. Such waves describe local fields in the far zone of a source that propagate as $1/r$ with distance. Above an interface with low normalized impedance, the direct and reflected modes rapidly cancel below the Brewster angle, leaving a radiated field that has been referred to as the "Norton surface wave" above a flat homogeneous medium [26]–[28], "lateral waves" above stratified media [29], and the "diffracted field" near and below the horizon of a spherical earth interface [28], [30], [31]. *In all cases, these forms of surface-wave fields do not follow the* $1/r$ *distance dependence from the source.*

Focusing our attention on the above example (VV backscatter above the sea at HF), the following two-step procedure is outlined to calculate the backscattered power level: 1) use the appropriate method to explain the propagation from the radar source to and from the sea cell (e.g., residue series [30])

and 2) take the surface within the cell to be locally perfectly conducting and use the resulting perturbation α^0 backscatter law for σ°. Although this seems to justify the α^0 law, which we have just shown to fail for plane wave backscatter, the arguments below suggest how it becomes reasonable when propagation is grouped together with scatter.

a) Propagation to the cell: Barrick [5] applied the compensation theorem of Monteath [23], [24] to VV surface wave backscatter from the sea at HF. We review the procedure here in order to justify the "perfectly conducting" assumption for the backscatter return. This integral-equation form of the compensation theorem expresses the "perturbed" field at an observation point due to scatter from a surface cell in terms of an "unperturbed" re-radiating source at the same point. The equation is integrated over the imperfect surface with normalized impedance Z. The "unperturbed source" produces its field at the observation point above a perfectly conducting surface; for a vertical dipole re-radiator near the surface, this is the sum of its free-space and image fields. Solution of the integral equation for the "perturbed" field then corrects the unperturbed field by the Norton surface-wave attenuation factor. In other words, without invoking the Sommerfeld radiation integrals, one ends up with the same result by another route, starting with re-radiation above perfectly conducting media.

Instead of the dipole, replace it with a cell that re-radiates the vertically polarized field scattered by a perfectly conducting version of the sea roughness within the cell. One may think of this as a collection of vertical dipoles in the cell with the appropriate currents to excite the equivalent unperturbed fields. This unperturbed re-radiated field is generated by the *total* incoming vertical E-field from the transmitter arriving at the cell by a surface-wave mode. This unperturbed re-radiation then gets multiplied by a surface-wave attenuation factor that accounts for propagation back to the receiver.

Quantifying this approach, we write the "radar equation" as

$$P_R = \{P_T G_T\} \left\{ \frac{F_T^2}{4\pi R_T^2} \right\} \{\sigma_c^\circ A\} \left\{ \frac{F_R^2}{4\pi R_R^2} \right\} \left\{ \frac{\lambda^2 G_R}{4\pi} \right\} \tag{23}$$

where P_T, P_R are the transmitted received powers, G_T, G_R are the transmit receive antenna gains, R_T, R_R are distances from scatterer to the transmitter receiver, λ is the wavelength, σ_c° is the "unperturbed" target scatter cross section per unit area from a perfectly conducting sea profile, A is the area within the surface cell, and F_T, F_R are the "attenuation factors" accounting for other than free-space propagation along the two paths. The bracketing in the above equation separates the propagation factors (second and fourth) from the remainder. It is the factors F_T and F_R that are rigorously derived from the compensation theorem approach, based on using an unperturbed scatter cross section for a perfectly conducting rough interface.

b) Unperturbed re-radiation or scatter from the cell: The Appendix obtains perturbation theory expressions for scatter from our Section II modal formulation. Leaving the scatter and incidence angles (β, α) different for generality, we obtain the following version of the normalized 1-D bistatic scattering cross section for VV

$$\sigma^\circ = \pi k^3 S(\kappa_B) \left| \frac{\sin\alpha}{\sin\alpha + Z} \right|^2 |1 - \cos\alpha\cos\beta - Z^2|^2 \cdot \left| \frac{\sin\beta}{\sin\beta + Z} \right|^2. \tag{24}$$

Here, $S(\kappa_B)$ is the 1-D wave height spatial spectrum evaluated at the Bragg wavenumber. This result has critical dependences on finite surface impedance Z (which can include the roughness effects) as the first and third absolute-value factors. If one lets $Z = 0$, these factors become unity; this is the classic result for VV scatter from the perfectly conducting surface we referred to in the preceding section. Note the importance of the order for limits near grazing: if we take $\sin\alpha$ or $\sin\beta \Rightarrow 0$ first, the cross section is zero at grazing, and it is too late to then set $Z = 0$.

Cast in the above form, (24) when compared to (23) reveals a more satisfying definition of the "unperturbed" cross section as $\sigma_c^\circ = 4\pi k^3 S(\kappa_B)$ (after reducing to backscatter where $\cos\alpha = -\cos\beta \Rightarrow 1$ and $1 - \cos\alpha\cos\beta - Z^2 \Rightarrow 2$). The first and third squared factors are identically the attenuation functions required for plane-wave propagation if the effects of finite surface impedance are grouped with propagation rather than with scatter! For in this case, the sum of the direct and specularly reflected rays on a plane surface [divided by two to accommodate our definition in (23)] become

$$F_T = \left| \frac{1 + R_v(\alpha)}{2} \right| = \left| \frac{\sin\alpha}{\sin\alpha + Z} \right| \tag{25}$$

with an analogous expression for F_R in terms of β. Thus, when the plane wave picture no longer describes propagation near grazing, e.g., in the surface wave zone, one merely replaces these factors for plane wave propagation with the appropriate attenuation factor. This is an heuristic way of explaining the more rigorous compensation theorem approach discussed above.

VI. Conclusions

We set out to establish limiting dependencies of backscatter and effective surface impedance/admittance for propagation versus grazing angle. Our results show that backscattered power depends on grazing angle to the fourth power; the impedance and admittance are constant as grazing is approached. These relations hold true for both polarizations, for arbitrary surface materials (including perfect conductors), for all frequency/roughness scales, and for a single deterministic roughness profile as well as averages over surface ensembles.

The formulation employed here treated only 2-D scatter/propagation above 1-D surface profiles. An impedance/admittance boundary was assumed, of which a perfect conductor (or Neumann–Dirichlet boundary) is a limiting case. Finally, we considered only backscatter rather than arbitrary bistatic scatter. The latter was a chosen based on the overwhelming ubiquitousness of backscatter radars, but the extension to bistatic scatter is obvious: as either the

incidence or scattering angle alone approaches grazing, echo power decreases as grazing angle squared (6), (7). Finally, although unproven by the present approach, we are confident that our grazing angle behavior applies to more general 2-D rough surfaces and lower media with dielectric constants that are not amenable to impedance/admittance boundary condition treatment.

The failure of these simple grazing-angle laws to explain many observations from HF through microwave is due to the inadequacy of plane waves to represent radiation from sources in the region very near or below the horizon. When the propagation mode is properly separated from the scatter interaction, we showed that even seeming paradoxical observations can be properly interpreted. Perhaps the profusion of differing power-law claims based on measurements is due to lack of discrimination of near-grazing propagation modes (direct and reflected plane rays, surface/lateral waves).

Although our approach was primarily employed to establish general grazing-limit behavior, our simple angle-independent constants describing backscatter and propagation (20), (22) are useful in their own right. Instead of requiring re-calculation for each angle near grazing, these expressions allow a single numerical evaluation to serve the entire near-grazing region up to the Brewster angle.

Interesting phenomena can be produced by roughness. For VV over perfect conductors (Neumann boundary), we end up with Brewster-angle behavior (dip in the reflection coefficient) at a specific incidence angle. This can also happen for HH for larger roughness scales, where the effective normalized "admittance" drops below unity, as it did in our example plotted in Fig. 5. These are somewhat surprising results.

Appendix
Perturbation Limit Results

We apply perturbation theory to our modal formulation [8] for 1-D impedance/admittance profiles. This differs from the usual perturbation approaches [5], [19], in that the Rayleigh hypothesis (upgoing wave modes fitted directly to the rough boundary) is not invoked. Our solution is a two-step process: first we solve (3a) for the surface current/field modes (not directly determined in the conventional Rayleigh approach); then we substitute these into (3b) for the scattered-field modes. With the assumption of small heights in terms of wavelength, the $m = 0$ row of (3a) becomes

$$\begin{Bmatrix} \sin\alpha + \mathtt{z} \\ (\sin\alpha)/\mathtt{y} + 1 \end{Bmatrix} [1 - (k\sin\alpha)^2 \nu_0] S_0 + ik\sin\alpha \sum_{n\neq 0} \cdot \begin{Bmatrix} (1-\xi_n\cos\alpha)/\sin\alpha + \mathtt{z} \\ (1-\xi_n\cos\alpha)/(\mathtt{y}\sin\alpha) + 1 \end{Bmatrix} S_n z_{-n} + O(3) = 2\sin\alpha. \tag{A.1}$$

The upper/lower notation goes with VV/HH polarization. In what follows—as well as other perturbation approaches—kz_n is assumed small (and becomes the perturbation parameter), *but* $\sin\alpha$ *is not assumed to be excessively small*. Terms of order two and higher in the perturbation parameter are included. The mth row of (3a) becomes

$$ik\chi_m z_m \begin{Bmatrix} (1-\xi_m\cos\alpha)/\chi_m + \mathtt{z} \\ (1-\xi_m\cos\alpha)/(\mathtt{y}\chi_m) + 1 \end{Bmatrix} S_0 + \begin{Bmatrix} \chi_m + \mathtt{z} \\ \chi_m/\mathtt{y} + 1 \end{Bmatrix} S_m + ik\chi_m \sum_{n\neq 0,\, m} \cdot \begin{Bmatrix} (1-\xi_m\xi_n)/\chi_m + \mathtt{z} \\ (1-\xi_m\xi_n)/(\mathtt{y}\chi_m) + 1 \end{Bmatrix} z_{m-n} S_n + O(3) = 0. \tag{A.2}$$

Per normal perturbation approaches, we group terms in orders of smallness. In (A.1) the first term is of "zero" order, as is the right side. Hence, S_0 has zero-order and second-order parts only. One solves (A.1) for the zero-order part of S_0 and substitutes it into (A.2). The first two terms of (A.2) are then seen to be first order with the remainder second order and, therefore, all remaining S_n (for $n \neq 0$) are first order or higher. Solutions for the zeroth-order part of S_0 and the coefficients S_n are

$$S_0^{(0)} = \begin{cases} \dfrac{2\sin\alpha}{\sin\alpha + \mathtt{z}} \\ \dfrac{2y\sin\alpha}{\sin\alpha + \mathtt{y}} \end{cases}$$

$$S_n^{(1)} = -ikz_n \begin{cases} \dfrac{2\sin\alpha}{\sin\alpha + \mathtt{z}} \dfrac{1 - \xi_n\cos\alpha + \mathtt{z}\chi_n}{\chi_n + \mathtt{z}} \\ \dfrac{2\mathtt{y}\sin\alpha}{\sin\alpha + \mathtt{y}} \dfrac{1 - \xi_n\cos\alpha + \mathtt{y}\chi_n}{\chi_n + \mathtt{y}} \end{cases}. \tag{A.3}$$

We perform similar expansions and groupings of (3b). By inspection, the left sides are written from (A.1) and (A.2) above by changing the signs before $\mathtt{z}/\mathtt{y}$ and before i. Like (A.3), F_0 has zero-order and second-order parts while F_n is first order. Then S_0 and S_n from (A.3) are substituted into these equations and they are solved to give

$$F_0^{(0)} = \begin{cases} \dfrac{\sin\alpha - \mathtt{z}}{\sin\alpha + \mathtt{z}} \\ \dfrac{\sin\alpha - \mathtt{y}}{\sin\alpha + \mathtt{y}} \end{cases}$$

$$F_n^{(1)} = -ikz_n \begin{cases} \dfrac{2\sin\alpha}{\sin\alpha + \mathtt{z}} \dfrac{1 - \xi_n\cos\alpha - \mathtt{z}^2}{\chi_n + \mathtt{z}} \\ \dfrac{2\sin\alpha}{\sin\alpha + \mathtt{y}} \dfrac{1 - \xi_n\cos\alpha - \mathtt{y}^2}{\chi_n + \mathtt{y}} \end{cases}. \tag{A.4}$$

Several features are apparent in (A.4) above. To zero order, the forward mode from a slightly rough surface F_0 is identically the Fresnel reflection coefficient for a smooth plane (as originally noted by Rice [19]) and given earlier in (9). When we apply the geometry symmetry condition discussed in Section IV-B1) so that the integer backscatter mode becomes identically $n^* = 2k\cos\alpha/\kappa$, then F_{n^*} becomes

$$F_{n^*}^{(1)} = -ikz_{n^*} \begin{cases} \dfrac{2\sin\alpha}{\sin\alpha + \mathtt{z}} \dfrac{1 + \cos^2\alpha - \mathtt{z}^2}{\sin\alpha + \mathtt{z}} \\ \dfrac{2\sin\alpha}{\sin\alpha + \mathtt{y}} \dfrac{1 + \cos^2\alpha - \mathtt{y}^2}{\sin\alpha + \mathtt{y}}. \end{cases} \tag{A.5}$$

An obvious variation of this expression was used in (24) for bistatic scatter toward grazing angle β; in (A.5) for backscatter

$\beta = \pi - \alpha$, as contained in the index n^*. The reasons for the difficulties with perfectly conducting surfaces noted by Kim and Stoddart [3] can now be examined further. In this limit, $z \Rightarrow 0$ and $y \Rightarrow \infty$. There is no problem with HH as the final power is seen to vary as $\sin^4 \alpha$ when the F_{n^*} mode is substituted into (7). For VV, if we allow even an infinitesimal value for z, in the grazing limit we see that power from (7) or (24) also varies as $\sin^4 \alpha \Rightarrow \alpha^4$. If, however, the perfectly conducting condition (Neumann boundary) is applied from the outset so that $z = 0$, one ends up with the classic perturbation limit $(1 + \cos \alpha)^2$ versus grazing angle (as noted in [3]) and also the constant claimed by Tatarskii and Charnotskii [6] for Neumann boundaries of any scale. This is not a failing of perturbation theory, because if $z = 0$, then the first term and right side of (A.1) above vanish, thus failing the assumption that they are not small quantities, which underpins classic perturbation solutions and the work of Kim and Stoddart [3]. Hence, the above perturbation approach should simply never have been used for $z = 0$ because quantities assumed to be zero-order (i.e., the largest) in size actually vanish as $\alpha \Rightarrow 0$! The transition zone from nearly constant behavior at higher grazing angles toward an α^4 fall off at grazing for VV is seen in the example plotted in Fig. 2 earlier.

ACKNOWLEDGMENT

The author would like to thank Dr. W. J. Erwin, WJE Physics Consultants, San Jose, CA, for his careful checking of all of the derivations and proofs herein.

REFERENCES

[1] D. E. Barrick, "A review of scattering from surfaces with different roughness scales," *Radio Sci.*, vol. 3, pp. 865–868, 1968.
[2] G. T. Ruck, D. E. Barrick, W. D. Stuart, and C. K. Krichbaum, "Rough surfaces," in *Radar Cross Section Handbook.* New York: Plenum, 1970, vol. 2, ch. 9.
[3] M.-J. Kim and A. J. Stoddart, "The region of validity of perturbation theory," *Waves Random Media*, vol. 3, pp. 325–342, 1993.
[4] D. E. Barrick, "Theory of HF/VHF propagation across the rough sea—Parts I and II," *Radio Sci.*, vol. 6, pp. 517–533, 1971.
[5] ———, "First-order theory and analysis of MF/HF/VHF scatter from the sea," *IEEE Trans. Antennas Propagat.*, vol. AP-20, pp. 2–10, 1972.
[6] V. I. Tatarskii and M. Charnotskii, "On the behavior of scattering from a rough surface for small grazing angles," *IEEE Trans. Antennas Propagat.*, this issue, pp. 67–72.
[7] A. G. Voronovich, "On the theory of electromagnetic waves scattering from the sea surface at low grazing angles," *Radio Sci.*, vol. 31, pp. 1519–1530, 1996.
[8] W. T. Shaw, A. J. Dougan, and R. J. A. Tough, "Analytical expressions for correlation functions and Kirchhoff integrals for Gaussion surfaces with ocean-like spectra," *IEEE Trans. Antennas Propagat.*, vol. 44, pp. 1454–1463, 1996.
[9] F. E. Nathanson, J. P. Reilly, and M. N. Cohen, *Radar Design Principles, Signal Processing, and the Environment.* New York: McGraw-Hill, 1991, pp. 275–278.
[10] D. B. Trizna and D. J. Carlson, "Studies of dual polarized low grazing angle radar sea scatter in nearshore regions," *IEEE Trans. Geosci. Remote Sensing*, vol. 34, pp. 747–757, 1996.
[11] P. H. Y. Lee, J. D. Barter, K. L. Beach, C. L. Hindman, B. M. Lake, H. Rungaldier, J. C. Shelton, A. B. Williams, R. Yee, and H. C. Yuen, "X band microwave backscattering from ocean waves," *J. Geophys. Res.*, vol. 100, pp. 2591–2611, 1995.
[12] L. B. Wetzel, "Sea clutter," in *Radar Handbook*, M. I. Skolnik, Ed., 2nd. ed. New York: McGraw-Hill, 1990, pp. 13.1–13.40.
[13] J. R. Wait, *Electromagnetic Waves in Stratified Media.* New York: Pergamon, 1962, p. 372.
[14] ———, "On the theory of radio propagation over a slightly roughened curved earth," in *Electromagnetic Probing in Geophysics*, J. R. Wait, Ed. Boulder, CO: Golem, 1971, pp. 370–381.
[15] E. Feynberg, "On the propagation of radio waves along an imperfect surface," *J. Phys. (Moscow)*, vol. 9, pp. 317–330, 1944.
[16] G. D. Dockery and J. R. Kuttler, "An improved impedance-boundary algorithm for Fourier split-step solutions of the parabolic wave equation," *IEEE Trans. Antennas Propagat.*, vol. 44, pp. 1592–1599, 1996.
[17] A. R. Miller, R. M. Brown, and E. Vegh, "New derivation for the rough-surface reflection coefficient and for the distribution of sea-wave elevations," *Proc. Inst. Elect. Eng.*,, vol. 131, pt. H, pp. 114–116, 1994.
[18] D. E. Barrick, "Near-grazing illumination and shadowing of rough surfaces," *Radio Sci.*, vol. 30, pp. 563–580, 1995.
[19] S. O. Rice, "Reflection of electromagnetic waves from slightly rough surfaces," in *Theory of Electromagnetic Waves*, M. Kline, Ed. New York: Wiley, 1951, pp. 351–378.
[20] W. H. Peake, "Theory of radar return from terrain," *IRE Int. Conv. Record*, vol. 7, pt. 1, pp. 27–41, 1959.
[21] D. E. Barrick, "The interaction of HF/VHF radio waves with the sea surface and its implications," in *Electromagn. Sea, AGARD Conf. Proc.*, Springfield, VA, 1970, Accession AD716305, pp. 18-1–18-25.
[22] P. Beckmann and A. Spizzichino, *The Scattering of Electromagnetic Waves from Rough Surfaces.* New York: Pergamon, 1963.
[23] G. D. Monteath, "Application of the compensation theorem to certain radiation and propagation problems," *Proc. Inst. Elect. Eng.*, vol. 98, pp. 23–30, 1951.
[24] R. J. King, "Electromagnetic propagation over a constant impedance plane," *Radio Sci.*, vol. 4, pp. 255–268, 1969.
[25] D. Holliday, L. L. DeRaad, and G. J. St-Cyr, "Volterra approximation for low grazing angle shadowing on smooth ocean-like surfaces," *IEEE Trans. Antennas Propagat.*, vol. 43, pp. 1199–1206, 1995.
[26] K. A. Norton, "Physical reality of space and surface waves in the radiation field of radio antennas," *Proc. IRE*, vol. 25, pp. 1192–1202, 1937.
[27] ———, "The propagation of radio waves over the surface of the earth and in the upper atmosphere," *Proc. IRE*, vol. 25, pp. 1203–1236, 1937.
[28] J. R. Wait, *Electromagnetic Waves in Stratified Media.* New York: MacMillan, 1962, ch. 2, 5.
[29] R. W. P. King, M. Owens, and T. T. Wu, *Lateral Electromagnetic Waves.* New York: Springer-Verlag, 1992, p. 746.
[30] V. A. Fock, *Electromagnetic Diffraction and Radiation Problems.* New York: Pergamon, 1965, pt. 1, p. 414.
[31] D. A. Hill and J. R. Wait, "Ground wave attenuation for a spherical earth with arbitrary surface impedance," *Radio Sci.*, vol. 15, pp. 637–643, 1980.

Donald E. Barrick was born in Tiffin, OH. He received the B.E.E., M.Sc., and Ph.D. degrees in electrical engineering from The Ohio State University, Columbus, OH.

He joined the staff of Battelle Memorial Institute, Columbus, OH, 1965, where he led work in radar scattering and signal processing as an Institute Fellow until 1972. During this time he taught electromagnetics and communications theory in the Electrical Engineering Department, The Ohio State University, as an Adjunct Assistant Professor. From 1972 to 1982 he served as Chief of the Sea State Studies Division of the U.S. National Oceanic and Atmospheric Administration's Wave Propagation Laboratory, Boulder, CO. There he developed compact HF radar systems for real-time mapping of ocean currents and waves. Since 1982 he has worked in industry, founding and heading CODAR Ocean Sensors, Ltd., Los Altos, CA, as President. In 1987 he joined Acurex Corporation, Mountain View, CA (part time) as Manager of the Electromagnetics Department. From 1989 to 1992 he served part time as Chief Scientist for Mirage Systems, Sunnyvale, CA. He has published over 130 papers in the open literature and co-authored several books, including *Radar Cross Section Handbook (Vols. I and II)* (New York: Plenum, 1970). His interests and experience include radio wave propagation and scatter above the earth at lower frequencies and development of compact low-frequency radar systems with novel waveforms, leading to several U.S. patents.

Dr. Barrick is a member of Sigma Xi, URSI Commissions F and C, the American Geophysical Union, and the American Meteorological Society. He has served as Associate Editor and Administrative Committee member for IEEE Antennas and Propagation Society.